

FEM MODELING OF REBAR CORROSION – NUMERICAL VERIFICATION OF EXPERIMENTAL RESEARCH

Tomasz KRYKOWSKI

Silesian University of technology, Faculty of Civil Engineering,
ul. Akademicka 5, 44-100 Gliwice, Poland

tomasz.krykowski@polsl.pl

The paper presents the experimental verification of concrete cover splitting time theory based on the multicomponent media approach and FEM. The results of computer analysis are compared with the experiment presented in the work of Youping Liu [15]. The solid model of the structure analyzed in the paper [15] has been made. The problem has been analyzed by using the program for the elastic plastic analysis with distortions by using FEM.

Keywords: corrosion, theory of plasticity, FEM, reinforced concrete degradation

1. INTRODUCTION

The pollution of the environment influences the reinforced concrete structures durability in a significant way. The aggressive substances such as all types of acid anhydride, chloride and ammonium ions evoke corrosion of steel and concrete. This subject area, in terms of high repair and damage costs, meets with wide interest of scientists of different types of knowledge. The problem of metal corrosion is the subject matter of various types of scientific works [23, 27, 31]. In terms of reinforced concrete elements the direct transfer of metal corrosion results is not possible [32]. This results from a peculiarity of concrete structures, steel concrete connections and processes occurring in this highly inhomogeneous capillary porous media. The characteristic feature of concrete pores is open porosity [21]. The system of pores, through which a transport of aggressive substance, liquids, gases in and out of concrete, is possible. In well designed reinforced concrete structures, having the cover of correct thickness, rebar corrosion should not appear for dozens of years. The time of safe structure using is associated with the designed cover thickness. The cover should

guarantee that the corrosion processes will not be found in the structure before the calculated durability time. The durability time is usually defined as a two stage process [26]. In the description of two stage process the following phases can be pointed out: initiation and structure degradation. A better method of structures durability description is the three stage process - the approach that can be found in the following papers [4, 21, 22, 24, 25], fig. 1. The first stage describes the aggressive substance transport [6, 28, 33] which is finished by initiation of corrosion process. The second stage is the mechanical degradation process of concrete cover as the result of corrosion products creation on the rebar surface. The third stage is initiated in the moment of concrete cover fracturing. In this stage the rate of structure degradation is relatively rapid because of the non limited oxygen supply to the cell.

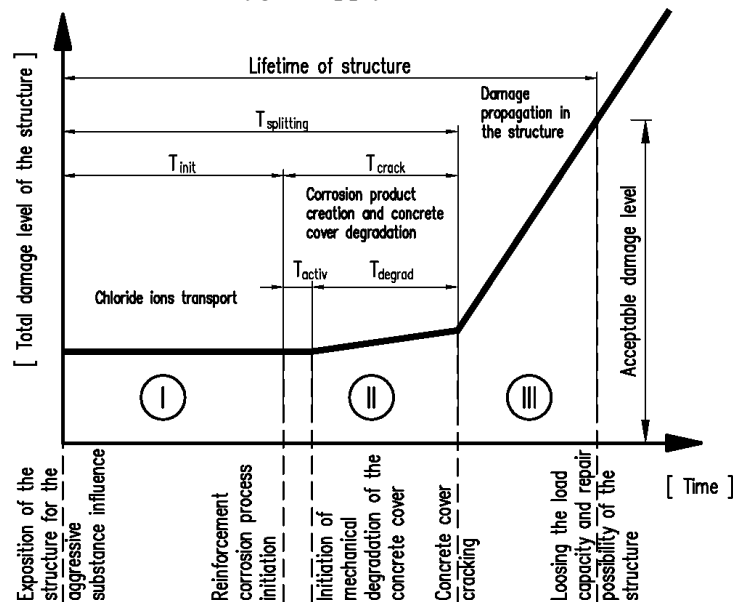


Fig. 1. Three stage model of reinforced concrete elements degradation as the result of rebar's corrosion

In the three stage model the very important problem is determination of the time $T_{crack} = T_{activ} + T_{degrad}$ followed by the fracture of concrete cover. The time T_{activ} is the time of concrete pores filling by the corrosion products, and T_{degrad} the time from the moment of concrete pores filling to cover cracking.

In this paper the comparison of computational results of the concrete cover fracturing time T_{crack} with the experimental results has been made. The computer calculations presented in [9], were carried with the aid of FEM based on the multicomponent media theory.

2. BACKGROUND OF CALCULATION METHOD

The concrete cover cracking time T_{crack} can be determined by using the method presented in paper [9]. The model showed in these papers assumes that the degradation of the cover as the result of rebar's corrosion can be described by using theory of multicomponent media [3, 5, 11, 29, 30, 32]. Assuming the four component model the mass balance equations: skeleton $\alpha=0$, aggressive substance $\alpha=1$, substrates $\alpha=2$ and corrosion products $\alpha=3$ will have the following form

- Mass balance of the skeleton

$$\rho \frac{d}{dt}(c^0) = 0, \quad (2.1)$$

- Mass balance of the aggressive substance

$$\rho \frac{d}{dt}(c^1) + \text{div}(\mathbf{j}^1) = 0, \quad (2.2)$$

- Mass balance of corrosion products and substrates

$$\rho \frac{d}{dt}(c^2) = \tilde{c}^2(I^e), \quad \rho \frac{d}{dt}(c^3) = \tilde{c}^3(I^e), \quad \tilde{c}^3(I^e) = -\tilde{c}^2(I^e), \quad I^e = \int_0^t I(\tau) d\tau \quad (2.3)$$

where ρ is the density of the media, c^0 is the concentration of the skeleton, c^1 is the aggressive substance concentration, \mathbf{j}^1 is the mass flux of aggressive substance, c^2 is the concentration of substrates, c^3 is the concentration of corrosion products, \tilde{c}^α is mass source productivity of substrates $\alpha=2$ and corrosion products $\alpha=3$, $I^e = I^e(I)$ is the function of corrosion current intensity I . Using the mass balance equation and average momentum, energy and entropy balance equation of the multicomponent media [9] and assuming the free Helmholtz [17, 20, 29, 30, 32] energy in the form

$$\psi = \psi(c^0, c^1, c^2(I^e), c^3(I^e), \boldsymbol{\varepsilon}^e, \boldsymbol{\alpha}, T) = \psi(c^0, c^1, \boldsymbol{\varepsilon}^e, \boldsymbol{\alpha}, I^e, T), \quad (2.4)$$

where $\boldsymbol{\varepsilon}^e$ is tensor of elastic strains, $\boldsymbol{\alpha}$ internal plastic parameter, T common temperature for all of the components the residual inequality will have the form

$$\left(-\rho \frac{\partial \psi}{\partial \boldsymbol{\varepsilon}^e} + \boldsymbol{\sigma} \right) : \dot{\boldsymbol{\varepsilon}}^e + \left(-\rho \frac{\partial \psi}{\partial T} - \rho s \right) \dot{T} + \left(-\rho \frac{\partial \psi}{\partial c^1} + \rho M^1 \right) \dot{c}^1 + \mathbf{D} \geq 0, \quad (2.5)$$

$$\mathbf{D} = \boldsymbol{\sigma} : \dot{\boldsymbol{\varepsilon}}^p - \mathbf{X}^\alpha \bullet \dot{\boldsymbol{\alpha}} - X^I \dot{I}^e - \mathbf{j}^1 \cdot \text{grad}(M^1) - \frac{\mathbf{q} \cdot \text{grad}(T)}{T} \geq 0. \quad (2.6)$$

where $\boldsymbol{\varepsilon}^p$ is plastic strain tensor. Assuming the isothermal condition the constitutive relationships for elastic – plastic material with mechanical distortions and transport of the aggressive substance [9] will have the form

$$\dot{\boldsymbol{\sigma}} = \rho \frac{\partial^2 \psi}{\partial \boldsymbol{\varepsilon}^e{}^2} : \dot{\boldsymbol{\varepsilon}}^e = \mathbf{C}^{ep} : (\dot{\boldsymbol{\varepsilon}} - \boldsymbol{\chi} \dot{I}^e), \quad (2.7)$$

$$\rho M^1 = \rho \frac{\partial \psi}{\partial c^1} = \rho M^1(c^1). \quad (2.8)$$

where \mathbf{C}^{ep} is material elastic tensor, $\boldsymbol{\chi}$ corrosion expansion tensor. Introducing [12, 18] the thermodynamical potential function

$$\Theta = \Theta_m(\boldsymbol{\sigma}, \mathbf{X}^a) + \Theta_c(\mathbf{X}^I) + \Theta_d(\text{grad } M^1), \quad (2.9)$$

the evolution equations of internal parameters that fulfill the inequality (2.6) will have the form

$$\dot{\boldsymbol{\varepsilon}}^p = \gamma \frac{\partial \Theta_m(\boldsymbol{\sigma}, \mathbf{X}^a)}{\partial \boldsymbol{\sigma}}, \quad (2.10)$$

$$-\dot{\boldsymbol{a}} = \gamma \frac{\partial \Theta_m(\boldsymbol{\sigma}, \mathbf{X}^a)}{\partial \mathbf{X}^a}, \quad (2.11)$$

$$-\dot{I}^e = \frac{\partial \Theta_c(\mathbf{X}^I)}{\partial \mathbf{X}^I}, \quad (2.12)$$

$$-\dot{\mathbf{j}}_1 = \frac{\partial \Theta_d(\text{grad } M^1)}{\partial (\text{grad } M^1)}. \quad (2.13)$$

Using aggressive substance mass balance equation (2.2), averaged momentum balance equation and performing linearization of these relationships [9] the linearized weak form of balance equations that can be solved by using FEM will be obtained. Introducing the approximation of displacement and concentration field

$$c \approx c^h(\mathbf{x}) = \bar{\mathbf{N}}(\mathbf{x}) \bar{\mathbf{c}}, \quad \mathbf{u} \approx \mathbf{u}^h(\mathbf{x}) = \bar{\mathbf{N}}(\mathbf{x}) \bar{\mathbf{u}} \quad (2.14)$$

where $\bar{\mathbf{N}}(\mathbf{x})$ is matrix of the shape functions, $\bar{\mathbf{c}}$ and $\bar{\mathbf{u}}$ are vectors of concentration and displacement respectively we will have the following formulas:

The equation describing the transport of aggressive substances in concrete

$$\frac{1}{\Delta t} (\bar{\mathbf{C}}_{n+1} - \bar{\mathbf{K}}_{n+1}) \cdot \bar{\mathbf{c}}_{n+1} = \bar{\mathbf{R}}_{n+1} + \frac{1}{\Delta t} \bar{\mathbf{C}}_n \cdot \bar{\mathbf{c}}_n, \quad (2.15)$$

$$\bar{\mathbf{C}} = \int_{B^h} \bar{\mathbf{N}}^T \cdot \bar{\mathbf{N}} dB, \quad \bar{\mathbf{K}} = \int_{B^h} \frac{\partial \bar{\mathbf{N}}^T}{\partial \mathbf{x}} \cdot \mathbf{k}_D \cdot \frac{\partial \bar{\mathbf{N}}}{\partial \mathbf{x}} dB, \quad \bar{\mathbf{R}} = \int_{B^h} \bar{\mathbf{N}}^T \cdot \bar{j} dB, \quad (2.16)$$

where \bar{j} is the mass flux on the boundary, \mathbf{k}_D – diffusion tensor.

- The equation describing the mechanical degradation of the cover as the result of mechanical distortions caused by corrosion products creation

$$\bar{\mathbf{K}}_{n+1}^k d\Delta \bar{\mathbf{u}}_{n+1}^{k+1} - \bar{\mathbf{Q}}_{n+1}^k d\Delta I_{n+1}^{e^{k+1}} = \bar{\mathbf{F}}_{n+1}^{ext} - \bar{\mathbf{F}}_{n+1}^{int^k}, \quad d\Delta I_{n+1}^{e^{k+1}} = I(t_{n+1}^{k+1}) d\Delta t_{n+1}^{k+1}, \quad (2.17)$$

$$\bar{\mathbf{K}}_{n+1}^k = \int_{B^h} \bar{\mathbf{B}}^T \cdot \bar{\mathbf{C}}^{ep}|_{n+1}^k \cdot \bar{\mathbf{B}} dB, \quad \bar{\mathbf{Q}}_{n+1}^k = \int_{B^h} \bar{\mathbf{B}}^T \cdot \bar{\mathbf{C}}^{ep}|_{n+1}^k \cdot \bar{\chi} dB, \quad (2.17)$$

$$\bar{F}_{n+1}^{ext} = \int_{B^h} \bar{\mathbf{B}}^T \cdot \rho \bar{\mathbf{b}}_{n+1} dB + \int_{B^h} \bar{\mathbf{B}}^T \cdot \bar{\mathbf{p}}_{n+1} dB, \quad \bar{F}_{n+1}^{int^k} = \int_{B^h} \bar{\mathbf{B}}^T \cdot \bar{\boldsymbol{\sigma}}_{n+1}^k dB, \quad (2.18)$$

$$\bar{\mathbf{C}}_{n+1}^{ep}|_{n+1}^k = \frac{\partial \bar{\boldsymbol{\sigma}}}{\partial \bar{\boldsymbol{\varepsilon}}}|_{n+1}^k = - \frac{\partial \bar{\boldsymbol{\sigma}}}{\partial \bar{\boldsymbol{\varepsilon}}^d}|_{n+1}^k, \quad \bar{\mathbf{u}}_{n+1}^{k+1} = \bar{\mathbf{u}}_{n+1}^k + d\Delta \bar{\mathbf{u}}_{n+1}^{k+1}, \quad \bar{\mathbf{u}}_{n+1}^0 = \bar{\mathbf{u}}_n. \quad (2.19)$$

where $\bar{\mathbf{B}}$ is matrix of differential operators.

3. CORROSION EXPANSION COEFFICIENT

The numerical analysis of the problem requires a formulation of material corrosion expansion tensor $\boldsymbol{\chi}$. This parameter can be determined on the basis of analytical considerations [9, 10] by using the relationships between the amount of corrosion products and the amount of ferrous ions transferred into the pore solution. The rate of ferrous ions transfer into the pore solution can be described by using the Faraday's law

$$\dot{m}_{Fe^{2+}} = kI = kI^e \quad (3.1)$$

where $m_{Fe^{2+}}$ is the mass of ferrous ions transferred into the pore solution, k electrochemical equivalent of iron. It will be assumed that the ratio of mass and ferrous ions density transferred into the pore solution to mass and density of the corrosion products is constant. Assuming that the chemical composition of corrosion products is a function of $\text{Fe}(\text{OH})_3$ and $\text{Fe}(\text{OH})_2$ [1, 14, 15, 19] we will obtain

$$m_R = \frac{m_{Fe^{2+}}}{\alpha}, \quad \alpha_{Fe(\text{OH})_3} = 0.523, \quad \alpha_{Fe(\text{OH})_2} = 0.622, \quad (3.2)$$

$$\rho_R = \frac{\rho_{Fe^{2+}}}{\gamma}, \gamma_{Fe(OH)_3} = 2.09, \gamma_{Fe(OH)_2} = 2.24. \quad (3.3)$$

Effective in the mechanical sense corrosion products volume $V_{R,eff}$, causing the corrosion distortion can be defined [2, 16] in the form

$$V_{R,eff} = V_R - V_{Fe^{2+}} \quad (3.4)$$

where V_R is the corrosion products volume, $V_{Fe^{2+}}$ the volume of ferrous ions transferred into the pore solution. After taking into consideration equations (3.1), (3.2), (3.3), (3.4) the following equation will be obtained

$$\dot{V}_{R,eff} = \frac{\dot{m}_{Fe^{2+}}}{\rho_{Fe^{2+}}} (\alpha^{-1} \gamma - 1), \dot{m}_{Fe^{2+}} = k i^e, I^e = \int_0^t I(t) dt, i_{corr} = I \cdot S_c \cdot L_c \quad (3.5)$$

where i_{corr} is the corrosion current density, S_c is the length of arc with active corrosion processes, L_c is the length of reinforcement with active corrosion process, $A_c = L_c \cdot S_c$ is the surface area of the rebar with active corrosion process. It is usually assumed that $S_c = \pi \cdot D$ where D is the rebar diameter. Using the equation (3.5) the tensor of distortional strain can be presented [9] in the form

$$\dot{\boldsymbol{\varepsilon}}^d = \boldsymbol{\chi} \dot{I}^e, \boldsymbol{\chi} = \mathbf{1} \frac{\dot{V}_{R,eff}}{3V_0} = \mathbf{1} \frac{k(\alpha^{-1} \gamma - 1)}{3V_0 \rho_{Fe^{2+}}}, \mathbf{1} = \delta_{ij} \mathbf{e}_i \otimes \mathbf{e}_j, V_0 = S_0 \cdot L_c, \quad (3.6)$$

where S_0 is the cross section area of the active part of transition region surface [9, 10]. The initiation time of process of the concrete cover mechanical degradation from the moment of electrochemical corrosion activation to entire filling of pores free space can be determined from the equation [14, 15]

$$t_{activ} = \frac{\pi D w_p \rho_R L_c}{kI}, I = const \quad (3.7)$$

where w_p is the width of the assumed porous zone around the rebar.

4. COMPUTATIONAL EXAMPLE

The results of computer analysis were verified by using the Liu Youping [15] experiment. In this experiment among others the fracturing time of concrete cover in the model of bridge plate, fig. 1 has been analyzed. The concrete plate models with the chloride content 7.20 kg/m^3 , cover thickness 25 mm (1 in) and

0.0, 0.36, 0.71, 1.42, 2.85, 5.69 kg/m³ and concrete cover thickness 51 i 76 mm (2 and 3 inch) have been considered. Concrete cover thickness, measured after the cracking was respectively 27, 47 and 70 mm. The rebar’s diameter in the model that was the basis to verification of computer simulation was 0.625 in \cong 16 mm.

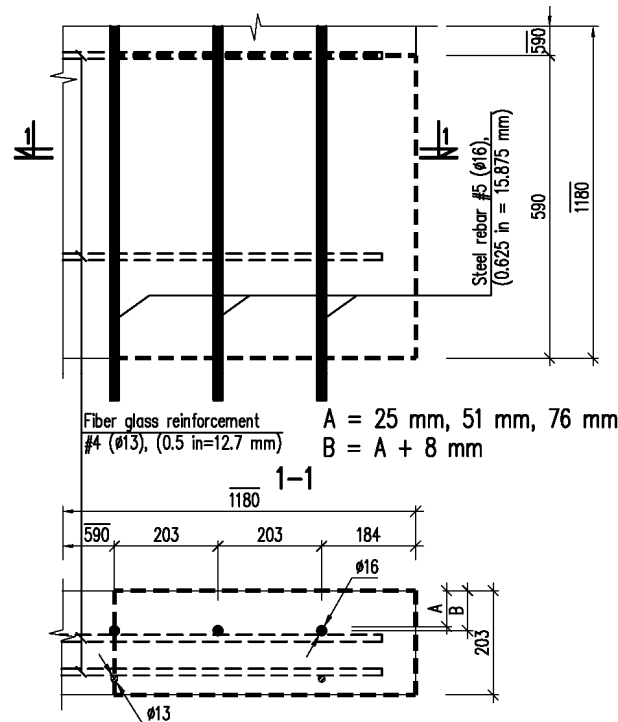


Fig. 2. The examined in Liu Youping experiment [15] reinforced concrete plate model

The top layer of reinforcement had 5 electrically insulated steel rebars in the longitudinal direction and three fiber glass #4 (12.7 mm) in the transverse direction. The bottom layer had three fiber glass rebar’s in both of directions. The reinforcement distribution in the analyzed plate has been presented on the fig. 2. The numerical verification has been executed in the simplified way by using the computer program for the analysis of elastic – plastic structures with mechanical distortions. The materials parameters and boundary conditions were applied similarly to the assumptions of the model work out in the paper [9]. The solid FEM model of the concrete deck plate has been made. The analysis has been made on 1/4 part of plate. The FEM model of the problem with shown rebar’s is presented on the fig. 3 (the model is inverted with respect to drawing shown on the fig. 2).

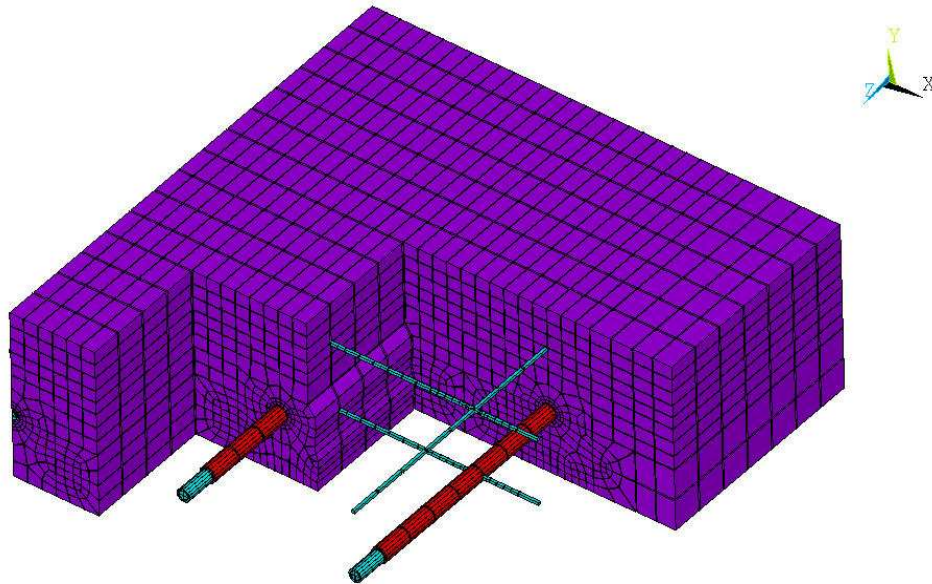


Fig. 3. FEM model of the concrete plate with shown rebar's and transition layer

The computer calculation have been made for the given in the paper [13, 14, 15] material parameters: the concrete compressive strength $f_{cm} = 31.5$ [MPa] = 4500 [psi], tensile strength $f_{ctm} = 3.3$ [MPa] = 4500 [psi], Young's modulus $E_s = 27$ [GPa] = 3900000 [psi], creep coefficient $\phi_{cr} = 2$, Poisson coefficient $\nu = 0.18$, corrosion products density $\rho_r = 3600$ [kg/m³] = 225 [lb/ft³], assumed effective width of porous zone $w_p = 12$ [μ m]. The required by the computer program parameters angle of internal friction and cohesive coefficient have been calculated on the basis of concrete strength in tension and compression $\Phi = 59.886$ [°], $c = 4.237 \cdot 10^6$ [N/m²], [7]. The Young's modulus used in the calculations was assumed in the form $E = E_s / (1 + \phi_{cr})$, [8]. The calculated values of the corrosion expansion coefficient are presented in the table 1. The concrete cover cracking time results are presented in the tables 2, 3, 4 respectively.

Table 1. The value of corrosion expansion coefficient (3.6) for the different values of α parameter depending on chemical composition of corrosion products: Fe(OH)₂, average value of α parameter and Fe(OH)₃ (average value is calculated for Fe(OH)₂ and Fe(OH)₃)

	Fe(OH) ₂ , $\alpha = 0.622$	$\alpha_{average} = 0.5725$	Fe(OH) ₃ , $\alpha = 0.523$
χ [1/(μ A·year)]	$343 \cdot 10^{-5}$	$385 \cdot 10^{-5}$	$434 \cdot 10^{-5}$

Table 2. The time of concrete cover fracturing T_{crack} [month], for the concrete cover thickness 25 and 27 mm, rebar diameter 16 mm, corrosion electric current density $i_{\text{corr}}=3.767368646$ [$\mu\text{A}/\text{cm}^2$] and corrosion electric current intensity $I=75.74744$ [μA]

Cover thickness / number of active elements	Model LW (Liu Y., Weyers R. [14,15]), $T_{\text{crack}}, \alpha = 0.622$	Model LW (Liu Y., Weyers R. [14,15]), $T_{\text{crack}}, \alpha = 0.523$	Activation time T_{activ} [14]	FEM model, $T_{\text{crack}}, \alpha = 0.622$	FEM model, $T_{\text{crack}}, \alpha = 0.5725$	FEM model, $T_{\text{crack}}, \alpha = 0.523$	Experiment result [14], T_{crack}
27 mm/ 4 active elements	6.75	9	1.5	4.75	5	5.5	8.5
25 mm/4 active elements	-----	-----	1.5	4.50	4.75	5.0	8.5
27 mm/16 active elements	6.75	9	1.5	5.25	5.75	6.25	8.5
25 mm/16 active elements	-----	-----	1.5	5.00	5.50	6.0	8.5

Table 3. The time of concrete cover fracturing T_{crack} [month], for the concrete cover thickness 47 and 51 mm, rebar diameter 16 mm, corrosion electric current density $i_{\text{corr}} = 2.346532471$ [$\mu\text{A}/\text{cm}^2$] and corrosion electric current intensity $I=47.17983$ [μA]

Cover thickness / number of active elements	Model LW (Liu Y., Weyers R. [14,15]), $T_{\text{crack}}, \alpha = 0.622$	Model LW (Liu Y., Weyers R. [14,15]), $T_{\text{crack}}, \alpha = 0.523$	Activation time T_{activ} [14]	FEM model, $T_{\text{crack}}, \alpha = 0.622$	FEM model, $T_{\text{crack}}, \alpha = 0.5725$	FEM model, $T_{\text{crack}}, \alpha = 0.523$	Experiment result [14], T_{crack}
47 mm/4 active elements	18.5	25.0	2.5	15.00	16.50	18.5	22
51 mm/4 active elements	-----	-----	2.5	19.00	21.00	23.0	22
47 mm/16 active elements	18.5	25.0	2.5	14.00	15.50	17.0	22
51 mm/16 active elements	-----	-----	2.5	15.50	17.00	18.5	22

Table 4. The time of concrete cover fracturing T_{crack} [month], for the concrete cover thickness 70 and 71 mm, rebar diameter 16 mm, corrosion electric current density $i_{\text{corr}}=1.79757304$ [$\mu\text{A}/\text{cm}^2$], and corrosion electric current intensity $I=36.14235$ [μA]

Cover thickness / number of active elements	Model LW (Liu Y., Weyers R. [14,15]), $T_{\text{crack}}, \alpha = 0.622$	Model LW (Liu Y., Weyers R. [14,15]), $T_{\text{crack}}, \alpha = 0.523$	Activation time T_{activ} [14]	FEM model, $T_{\text{crack}}, \alpha = 0.622$	FEM model, $T_{\text{crack}}, \alpha = 0.5725$	FEM model, $T_{\text{crack}}, \alpha = 0.523$	Experiment result [14], T_{crack}
70 mm/4 active elements	40.0	54.0	3.5	44.50	50.50	56.5	42.5
76 mm/4 active elements	-----	-----	3.5	56.50	62.50	69.5	42.5
70 mm/16 active elements	40.0	54.0	3.5	29.50	32.50	36.5	42.5
76 mm/16 active elements	-----	-----	3.5	33.50	36.50	40.5	42.5

In figure 4 the distribution of the results describing the dependence time to cover cracking versus the thickness of cover cracking has been shown. In figures 5, 6 the graphical view of the distribution of plastic equivalent strain in the concrete plate (51 mm thickness and 4 and 16 active elements respectively) and cross section 1-1 in the moment of cracking has been shown.

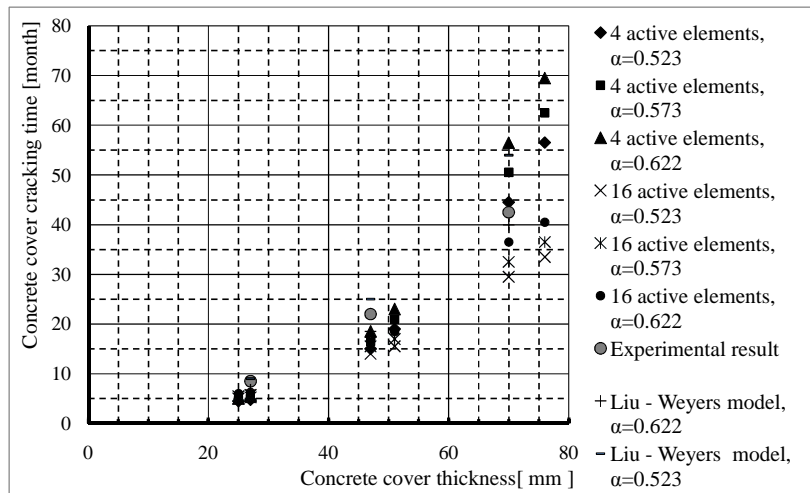


Fig. 4. Concrete cover thickness versus time to concrete cover cracking T_{crack}

```
ELEMENT SOLUTION
STEP=42
SUB =1
TIME=1.708
NLEPEQ (NOAVG)
RSYS=0
DMX =.235E-03
SMX =.033809
```

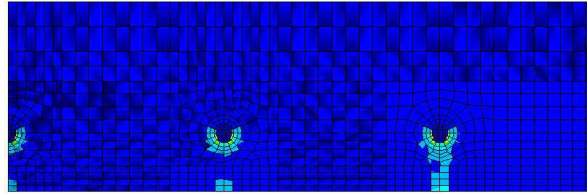


Fig. 5. The equivalent plastic strain distribution in the deck plate (concrete cover 51 mm and 4 active finite elements) in the moment of concrete cover cracking

```
ELEMENT SOLUTION
STEP=33
SUB =1
TIME=1.333
NLEPEQ (NOAVG)
RSYS=0
DMX =.590E-04
SMX =.001154
```

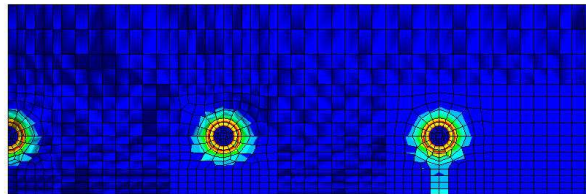


Fig. 6. The equivalent plastic strain distribution in the deck plate (concrete cover 51 mm and 16 active finite elements) in the moment of concrete cover cracking

5. SUMMARY AND FINAL PROPOSAL

Evaluating the obtained results of computer calculations we can find out that the times of concrete cover damage obtained in the computer analysis coincide with the experimental results. Specification is required for the determination of time of the pores filling by the corrosion product. The proposition (eqn. 3.7) taken from [15] is inconsistent with the concept of the presented model and requires further investigation.

ADDITIONAL INFORMATION

The paper has been prepared according to the grant number: POIG.01.01.02-10-106/09-00 Innovative Economy Program.

LITERATURE

1. Andrade C., Alonso C., Molina F. J.: *Cover cracking as a function of rebar corrosion: part I – experimental test*, Materials and Structures, Paris, **26**, 8 (1993) 453-464.
2. Bazant Z. P.: *Physical model for steel corrosion in concrete sea structures – theory*, Journal of the Structural Division ASCE, **105**, 6, (1979) 1137 – 1153.
3. Bowen R. M.: *Incompressible porous media model models by use of the theory of mixtures*, International Journal of Engineering Science, **18**, 9 (1980) 1129-1148.
4. Cady P.D., Weyers R.E.: *Deterioration rates of concrete bridge decks*, Journal of Transportation Engineering, **110**, 1 (1984) 34-44.
5. Černý R., Rovnaníková P.: *Transport processes in concrete*, London and New York, Spoon - Press 2002.
6. Chatterji S.: *On the applicability of Fick's second law to chloride ion migration through portland cement concrete*, Cement and Concrete Research, **25**, 2 (1995) 299-303.
7. Chen W. F., Zhang, H.: *Structural plasticity. Theory problems and CAE software*, New York, Springer-Verlag 1990.
8. Comite Euro-International Du Beton.: *CEB/FIP model code*, 1990.
9. Krykowski T.: *Modelling of concrete cover degradation caused by rebar's corrosion - multicomponent media theory approach*, Computer Assisted Mechanics and Engineering Sciences, **16**, (2009) 241-250.
10. Krykowski T., Zybura, A.: *Fem modeling of concrete cover degradation caused by rebars corrosion in reinforced concrete*, Architecture Civil Engineering Environment – ACEE Journal, **2**, 4 (2009) 71-80.
11. Kubik J.: *Thermodiffusion flows in a solid with a dominant constituent*, Mitteilungen aus dem Institut für Mechanik nr 44, Bochum, Ruhr-Universität Bochum 1995
12. Lemaitre J., Desmorat, R.: *Engineering damage mechanics, ductile, creep, fatigue and brittle failures*, Springer-Verlag 2005.
13. Liu T., Weyers R. W.: *Modeling the dynamic corrosion process in chloride contaminated concrete structures*, Cement and Concrete Research, **28**, 3 (1998) 365-379.
14. Liu Y., Weyers R. W.: *Modelling the time-to-corrosion cracking in chloride contaminated reinforced concrete structures*, ACI Materials Journal, **95**, 6 (1998) 675 – 680.
15. Liu Y.: *Modeling the time-to-corrosion cracking of the cover concrete in chloride contaminated reinforced concrete structures*, Ph.D. Thesis, Blacksburg, Virginia Polytechnic Institute and State University 1996.

16. Martín-Pérez B.: *Service life modelling of r.c. highway structures exposed to chlorides*, Ph.D. thesis, Department of Civil Engineering, University of Toronto, Toronto 1999.
17. Mase G. T., Mase G. E.: *Continuum mechanics for engineers*, Boca Raton - London - New York – Washington D. C, CRC Press 1999.
18. Maugin G. A.: *The thermomechanics of plasticity and fracture*, Cambridge, University Press 1992.
19. Pantazopoulou S. J., Papoulia K. D.: *Modeling cover-cracking due to reinforced corrosion in RC structures*, Journal of Engineering Mechanics, **127**, 4 (2001) 342 – 351.
20. Simo J.C., Hughes T. J. R.: *Computational inelasticity*, New York, Springer-Verlag 1998.
21. Ściślewski Z.: *Ochrona konstrukcji żelbetowych*, Warszawa, Arkady 1999.
22. Ściślewski Z.: *Problemy korozji w diagnostyce i przy wzmacnianiu konstrukcji żelbetowych*, Warszawa, Instytut Techniki Budowlanej 1994.
23. Shreir L. L.: *Korozja metali i stopów*, Warszawa, WNT 1966.
24. Suwito C., Xi Y.: *The effect of chloride-induced steel corrosion on service life of reinforced concrete structures*, Structure and Infrastructure Engineering, **4**, 3 (2006) 177 – 192.
25. Thoft-Christensen P.: *Corrosion and cracking of reinforced concrete*, in: *Proceedings of the 3rd IABMAS workshop on Life-Cycle Cost Analysis and Design of Infrastructure Systems*, ASCE (2003) 26-36.
26. Tuutti K.: *Corrosion of steel in concrete*, Swedish Cement and Concrete Research Institute, Stockholm 1982.
27. Uhlig H. H.: *Korozja i jej zapobieganie*, Warszawa, WNT 1976
28. Wieczorek G.: *Korozja zbrojenia inicjowana przez chlorki i karbonatyzację otuliny*, Wrocław, Dolnośląskie Wydawnictwo Edukacyjne 2002.
29. Wilmański K.: *Podstawy termodynamiki fenomenologicznej*, Warszawa, Państwowe Wydawnictwo Naukowe 1974.
30. Wilmański K.: *Continuum thermodynamics. part I: foundations*, Singapore, World Scientific 2008.
31. Wranglèn G.: *Podstawy korozji i ochrony metali*, Warszawa, WNT 1976.
32. Zybura A.: *Degradacja żelbetu w warunkach korozyjnych*, Z. 72, Gliwice, Zeszyty Naukowe Politechniki Śląskiej 1990.
33. Zybura A.: *Analysis of chloride migration in concrete based on multicomponent medium theory*, Archives of Civil Engineering, **53**, 1 (2007) 131-150.

MODELOWANIE MES KOROZJI ZBROJENIA – WERYFIKACJA NUMERYCZNA BADAŃ DOŚWIADCZALNYCH

Streszczenie

W pracy przedstawiono zastosowanie modelu bazującego na teorii ośrodków wieloskładnikowych i MES do wyznaczania czasu odspojenia otuliny betonowej. Wyniki analiz komputerowych porównano z wynikami eksperymentalnymi otrzymanymi w pracy [15]. Dla potrzeb analizy komputerowej wykonano model przestrzenny konstrukcji. Zagadnienie analizowano programem do obliczania konstrukcji w zakresie sprężysto plastycznym z dystorsjami mechanicznymi. Algorytm zaimplementowany w programie był modyfikowany stosownie do założeń teoretycznych modelu degradacji otuliny [9]. Jako wynik analizy otrzymano czas pęknięcia otuliny $T_{crack}=T_{activ}+T_{degrad}$, gdzie T_{degrad} jest czasem degradacji otrzymanym w wyniku analizy komputerowej natomiast czas aktywacji T_{activ} jest czasem wypełniania porów. Analizę komputerową przeprowadzono dla otulin grubości: 25, 51, 76 mm (1,2 3 [in] – projektowane grubości otulin) oraz dla 27, 47, 70 mm (1.07,1.84,2.74 [in] – rzeczywiste pomierzone grubości otulin). W wyniku przeprowadzonych obliczeń stwierdzono dobrą korelację wyników teoretycznych z wynikami eksperymentalnymi.